Primljen / Received: 14.2.2022.
Ispravljen / Corrected: 27.8.2022.
Prihvaćen / Accepted: 18.10.2022.
Dostupno online / Available online: 10.12.2022.

The Ultimate Bearing Capacity analysis of masonry arch bridges

Authors:

[1]**Kefan Chen**, MCE
kfchen@chd.edu.cn

[1,2] Assist.Prof. **Yuan Li**
2018121131@chd.edu.cn
Corresponding author

[1]**Qixiang Hui**, MCE
2020221027@chd.edu.cn

[3]**Bin Zhou**, MSc. CE
821499331@qq.com

[1]**Kang Wang**, MSc. CE
2020221005@chd.edu.cn

[1] University, Xi'an, China
Faculty of Transport
[1,2] Chang'an University, Xi'an, China
The main laboratory for the technology of detection and strengthening of old bridges of the Ministry of Transport
[3] Ningxia Communications Construction Co., China

Research Paper

Kefan Chen, Yuan Li, Qixiang Hui, Bin Zhou, Kang Wang

The Ultimate Bearing Capacity analysis of masonry arch bridges

To accurately evaluate the ultimate bearing capacity of masonry arch structures, considering the friction and bonding relationships between different components, a finite element model was established in this study with cohesive zero-thickness elements. The model was analysed using explicit dynamic simulations and verified through a case study. The results indicate that the thickness of the arch backfill and ring has a quadratic positive correlation with the ultimate bearing capacity of the structure, whereas the rise-span ratio has a cubic relationship. In particular, there is an optimal rise-span ratio (f/l = 1/3.909) to increase the bearing capacity of the structure under the same conditions.

Key words:
masonry arch structures, ultimate bearing capacity, finite element method, cohesive finite element, explicit dynamic analysis

Prethodno priopćenje

Kefan Chen, Yuan Li, Qixiang Hui, Bin Zhou, Kang Wang

Analiza granične nosivosti zidanih svođenih mostova

U svrhu točne procjene granične nosivosti zidanih lučnih konstrukcija, uzimajući u obzir odnos trenja i prionjivosti između različitih komponenti, u ovom je radu definiran numerički model metodom konačnih elemenata s kohezivnim elementima nulte debljine. Model je analiziran eksplicitnim dinamičkim simulacijama i potvrđen na stvarnom mostu. Rezultati pokazuju da je nosivost konstrukcije u pozitivnom kvadratnom omjeru s debljinom lučne ispune i prstena, a omjer visine i raspona mosta (strelica luka) imaju kubični omjer. Naime, postoji optimalna vrijednost strelice luka (f/l = 1/3,909), kod koje konstrukcija ima maksimalnu nosivost pod istim uvjetima.

Ključne riječi:
zidane lučne konstrukcije, granična nosivost, metoda konačnih elemenata, kohezivni konačni element, eksplicitna dinamička analiza

1. Introduction

Although masonry arch structures in civil engineering have been adopted since ancient times, predicting the bearing capacity of masonry arch structures is not an easy and clear task [1-3]. The structures account for most village road main parts or the part of the bridge cultural heritage. A detailed analysis of bearing capacity is important for their restoration, reinforcement, and preservation.

Most masonry arch structures have comprised blocks of various shapes and sizes and mortar joints since ancient times [4, 5]. These structures are primarily built using local materials with unknown material properties. Hence, the mechanism of the structures, especially the dynamic behaviour, is much more difficult to simulate accurately than that of prestressed concrete arch bridges [6]. In early research, the dynamic behaviour of masonry arch structures was investigated in depth by Jacques Heyman. With the development of computer and numerical methods, variable finite element models have been established using different elements, such as the finite element, discrete element, combining discrete element, and rigid body spring methods, to investigate the linear and nonlinear properties of structures [7-13]. Fang conducted three evaluation methods in American Association of State Highway and Transportation Officials and proposed a more accurate evaluation approach based on the load and resistance factor rating method [14]. Considering different contact interaction laws, Orduna conducted a detailed analysis of three-dimensional to examine the construction failure mechanism [15, 16].

It has been widely reported that the bearing capacity of masonry solid-web arch bridges is mostly defined by arch geometry, stone block dimensions, and interaction with the backfill material or surrounding walls [17-21]. As current bridge structures have better durability, the ultimate bearing capacity of actual structures is far beyond the expected value calculated by using conventional methods after considering the contribution of arch backfills, side walls, and abutments. If the actual ultimate bearing capacity in actual structures is inaccurate, the reinforced or rebuilt tasks of unqualified structures will be enormous and redundant. Therefore, with a large demand for the detection and reinforcement of masonry arch structures established on village roads, the development of the bearing capacity analysis of these structures must also be quantified.

Based on the experimental data from the reconstruction project in rural bridge reinforcement, considering the contribution of components and the friction between them to the bearing capacity, a finite element model was established with cohesive finite elements and analysed with an explicit dynamic simulation. The accuracy of the model was verified using a case study reported in the literature. On this basis, impact factors such as the rise-span ratio, thickness of the arch ring, and thickness of the backfill were discussed to provide a strong basis for the arch bridge bearing capacity for further study and evaluation.

2. Numerical methods of modelling

Generally, the constitutive relation of materials affects the macroscopic performance of structural material failures [22]. In this study, to accurately simulate the failure of a cohesive element, the bilinear constitutive relation [23] was applied (Figure 1).

In Figure 1, subscripts "n", "t" and "s" represent the parameters in the normal, tangential, and shear directions, respectively. The fractured form in tension in these directions corresponds to the opening mode (mode I), sliding mode (mode I), and anti-plane shear mode (mode II). The slopes of the trends in Figure 1, k_n and k_α (λ = t,s), are also the elastic stiffness in these three directions, as expressed in Eq. (1); σ_n and τ_λ τ_n are the tensile stresses in these three directions; σ_{max}, $\tau_{\lambda,max}$, τ_{max} are the maximum values of σ_n and τ_λ T_n respectively; δ_n^0 and δ_λ^0 are the corresponding displacement values of σ_n τ_λ, respectively; and δ_n^f and δ_λ^f are the ultimate cracked displacements in these three directions. The following equations for the constitutive relation can be obtained from Figure1:

$$k_n = \frac{\sigma_{max}}{\delta_n^0} \tag{1a}$$

$$k_\lambda = \frac{\tau_{\lambda,max}}{\tau_\lambda^0} \tag{1b}$$

$$\sigma_n = \begin{cases} k_n\delta & (\delta \le \delta_n^0) \\ \sigma_{max}\dfrac{\delta_n^f - \delta}{\delta_n^f - \delta_n^0} & (\delta > \delta_n^0) \end{cases} \tag{1c}$$

$$\tau_\lambda = \begin{cases} \mathrm{sgn}(\Delta u)\,k_\lambda\delta & (\delta \le \delta_\lambda^0) \\ \mathrm{gn}(\Delta u)\,\tau_{\lambda,max}\dfrac{\delta_\lambda^f - \delta}{\delta_\lambda^f - \delta_\lambda^0} & (\delta > \delta_\lambda^0) \end{cases} \tag{1d}$$

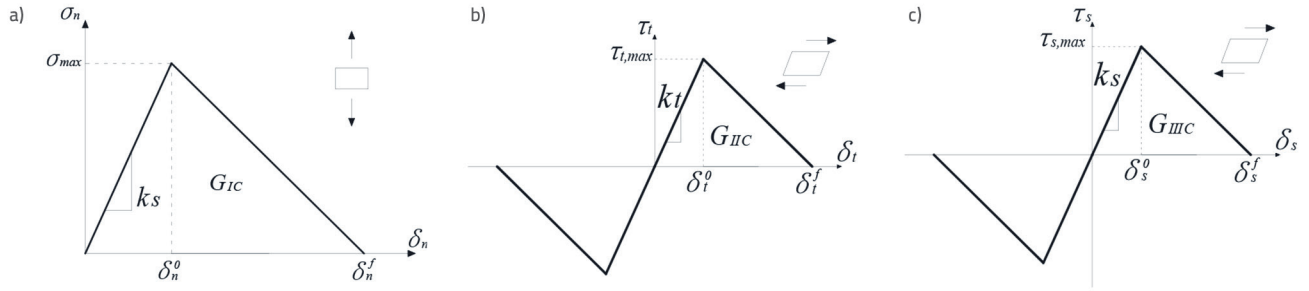

Figure 1. Bilinear constitutive relation: a) in normal direction; b) in tangential direction; c) in shear direction

Table 1. Instruction of the contact relationships

Connection type	Instruction
Tie	It is applied to couple two surfaces, where tension and pressure can be transmitted. The bound area will not undergo relative movement and deformation, and the rigidity is relatively large.
Coupling	It is applied to establish the constraint between the reference point and loading surface. The same rigid body motion occurs between the reference point and loading surface.
Cohesive	It is applied to simulate the sticky link between the two parts and the fracture of the material. It requires the size and strength of the bonding material to be smaller than the bonding part.
Friction	It is applied to simulate the tangential interaction between the filler and other bridge components. The tangent direction is controlled by friction, and the normal direction is simulated by 'hard contact' that allows separation, but prevents penetration, between contacting parts.

Thereafter, the fracture energy in these three modes can be obtained.

$$G_{IC} = \frac{1}{2}\sigma_{max}\delta_n^f \tag{2a}$$

$$G_{IIC} = \frac{1}{2}\tau_{t,max}\delta_t^f \tag{2b}$$

$$G_{IIIC} = \frac{1}{2}\tau_{s,max}\delta_s^f \tag{2b}$$

To accurately define the structural failure, the second nominal stress criterion was applied to determine the damage initiation when the stiffness of the structural material began to degrade, as expressed in Eq. (3):

$$D = \left\{\frac{\langle\sigma_n\rangle}{\sigma_{max}}\right\}^2 + \left\{\frac{\tau_t}{\tau_{t,max}}\right\}^2 + \left\{\frac{\tau_s}{\tau_{s,max}}\right\}^2 \tag{3a}$$

$$\langle\sigma_n\rangle = \begin{cases} 0 & \sigma_n \le 0 \\ \sigma_n & \sigma_n > 0 \end{cases} \tag{3b}$$

In Eq. (3b), the structural materials are not damaged under press, which is in line with the characteristics of stone arch bridge arch ring damage. After the damage started, a feature parameter for the fracture criterion G_{TC} was introduced with an initial value of 0. Therefore, the structural material is intact during G_{TC} = 0, whereas the structural material completely fails during G_{TC} = 1. Additionally, a fracture energy standard is applied to determine the failure of the structure. Specifically, the Benzeggagh-Kenane law was applied, as expressed in Eq. (4):

$$G_{TC} = G_{IC} + (G_{IIIC} - G_{IIC}) \cdot \left(\frac{G_{II} + G_{III}}{G_I + G_{II} + G_{III}}\right)^{\eta} \tag{4}$$

Where G_i (i = I, II, III) are the fracture energy in tension and η is a constant of the material that determines the response speed of material cracking and failure. Hence, the cohesive finite element adopted in this paper would be damaged by the stress. The opening displacement increases linearly with an increase in tension. When the tension reaches the peak value, the press gradually decreases linearly to zero an increase in the opening displacement. By referring to the parameter of G_{TC}, whether the material fails completely can be judged.

In this study, the interaction between the surfaces of different components was simulated using a nonlinear friction/bonding element [25, 26]. Four contact relationships were applied to the finite element model (Table 1).

Note that the viscous interaction of mortar between the ring and other bridge components is simulated by cohesive finite elements and the cohesive connection type, resulting in the following benefits:

- A unified constitutive relationship is adopted by the cohesive finite element to simulate the occurrence and development of cracks, reducing the probability of singular stress at the crack tip.
- The cohesion model can simulate a situation in which the crack tip enters plasticity, which provides an opportunity to study the state of large-scale yield at the crack tip.
- The cohesion model does not require preset cracks in the structure, and the solution process is relatively simple.
- The cohesion model can accurately simulate the damage initiation position and damage evolution process of a structure.

3. Explicit dynamic analysis and case verification

3.1. Parameters of the case study

By assembling the three-dimensional deformable parts determined by a C3D8R linear hexahedral 8-node element with six degrees of freedom for each node, the final geometric model of the structure is formed. The mortar was simulated by the bonding unit, whereas the bonding unit was simulated by the cohesive elements. To ensure the validity and accuracy of the cohesion model, explicit dynamic analysis was applied by referring to the detailed parameters from a loading test of a masonry arch bridge [26]. The masonry, stuffing, sidewall, and abutment components of the slab arch structure were simulated by solid elements using commercial software ABAQUS [27]. The adopted parameters are listed in Tables 2 and 3 [20, 26].

Table 2. Geometry parameters of the Cemetery Bridge [26]

Span [m]	**Rise** [m]	**RSR**	**TAR** [cm]	**Width of main arch ring** [m]	**TAS** [cm]
7.16	3.05	1/2.35	45	7.62	30

Table 3. Basic material properties of the Cemetery Bridge [26]

Component	**Yung's modulus** [MPa]	**Poisson ratio**	**Density** [kg/m^3]
Masonry	2400	0.2	2400
Stuffing	500	0.3	1750
Abutment	1500	0.2	2400

Table 4. Interface and boundary conditions of the model

Connection type	**Connection location**	
Tie	Arch ring	Side wall
	Abutment	Side wall
Coupling	1st reference point (loading)	Loading surface
Cohesive	Arch ring	Side wall
	Arch ring	Abutment
	Voids between blocks	
Friction	Arch ring	Stuffing
	Stuffing	Side wall
	Stuffing	Abutment

The bottom of the slab-arch bridge abutment is fully consolidated. Table 4 presents the other adopted contact relations, and Figure 2 shows a schematic summary of the modelling interface.

Table 5 presents the adopted parameters for the material property.

In Table 5, E_0 is Young's modulus of the masonry, f_t and f_s is the friction coefficient in two tangential directions. As previously mentioned, nonlinear friction/bonding elements were applied in this study to simulate the interaction between the backfill and other components in two tangential directions. Consequently, friction interaction was applied to the cohesive elements in the tangential and shear directions. The interaction in the normal direction was applied with hard contact, where the surface was allowed to separate and banned penetration. In addition, the stiffness in the normal direction k_n is adopted with a large number.

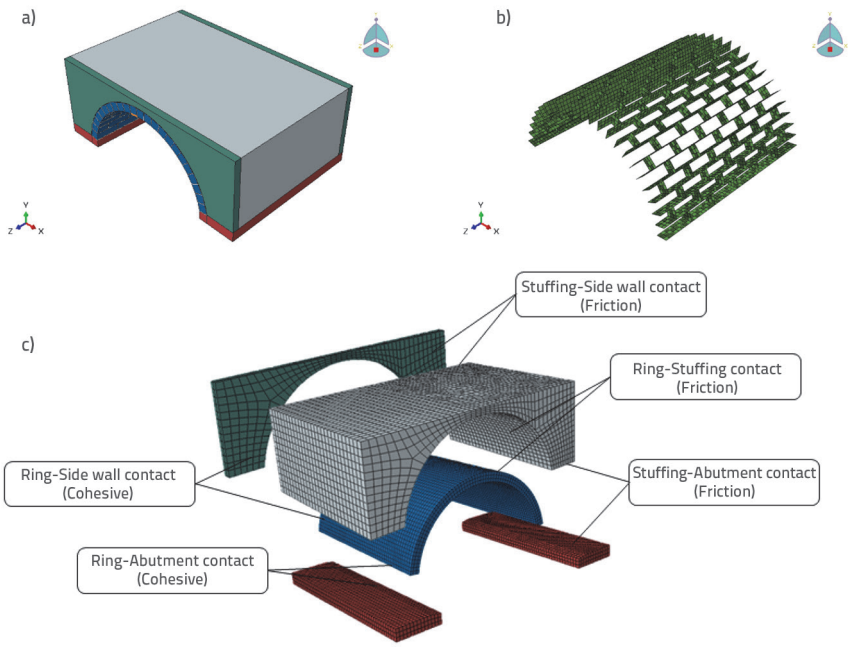

Figure 2. Finite element model with material interface types: a) Whole finite element model; b) Cohesive elements; c)Related interfaces of the whole finite model

Table 5. Parameters for the model

$\sigma_{n,max}$ [MPa]	$\tau_{t,max}$ [MPa]	$\tau_{s,max}$ [MPa]	G_I [N/mm]	G_{II} [N/mm]	G_{III} [N/mm]
0.051	0.063	0.063	0.02	0.125	0.125
k_n [MPa/mm]	k_t [MPa/mm]	k_s [MPa/mm]	η	f_t	f_s
$E_0 x 10^4$	3.98	3.98	2.2	0.3	0.3

To ensure a stable solution process of the quasi-static attribute, the smooth (mainly in the first and second derivatives) amplitude curve is applied with a 1 s loading time, which is approximately 10 times the natural vibration period (Figure 3).

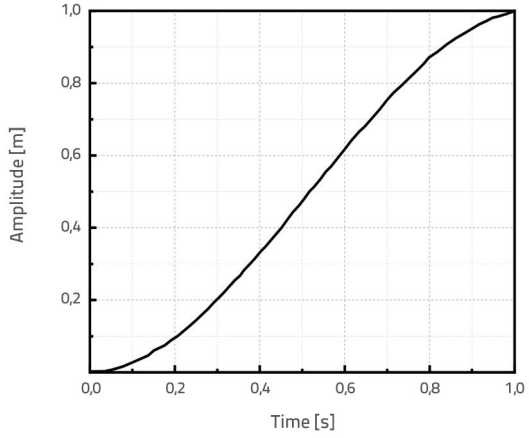

Figure 3. Smooth amplitude curve during 1.0 s

3.2. Explicit dynamic analysis

On the Cemetery Bridge, semi-load trucks were adopted for loading at the edge and centre of the road; full trucks were adopted for loading on the left and right sides of the road. Figure 4 presents the loading conditions of the Cemetery Bridge.
Note that the two longitudinal axes of the vehicle are equivalent to two loading blocks at the same cross-section (Figure 4).

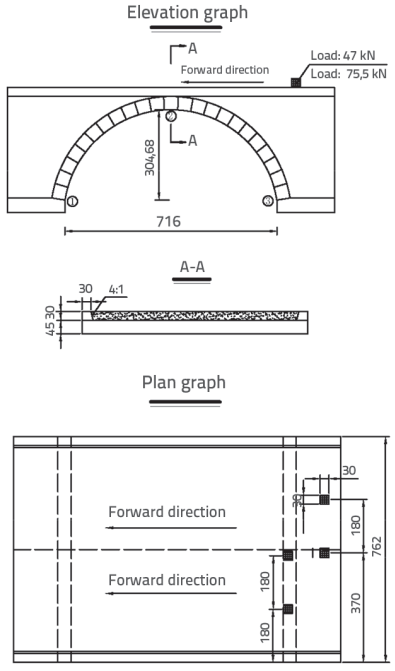

Figure 4. Parameters and loading conditions of the Cemetery Bridge

By comparing the energy time of the vehicle loading with the concentrated loading at the vault, it was verified that the dynamic simulation was quasi-static. Figure 5 shows the energy-time histories for these two conditions.
As shown in Figure 5, the kinetic energy in the vehicle loading does not exceed 3.2 % of the internal energy,

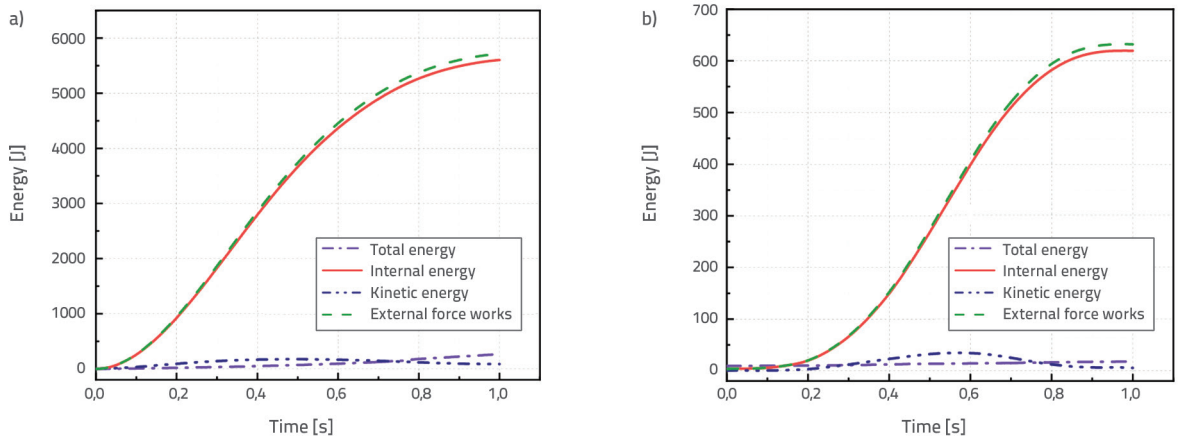

Figure 5. Energy-time histories analysis of the post-processing: a) Energy history while vehicle loading; b) Energy history while concentrated loading at the vault

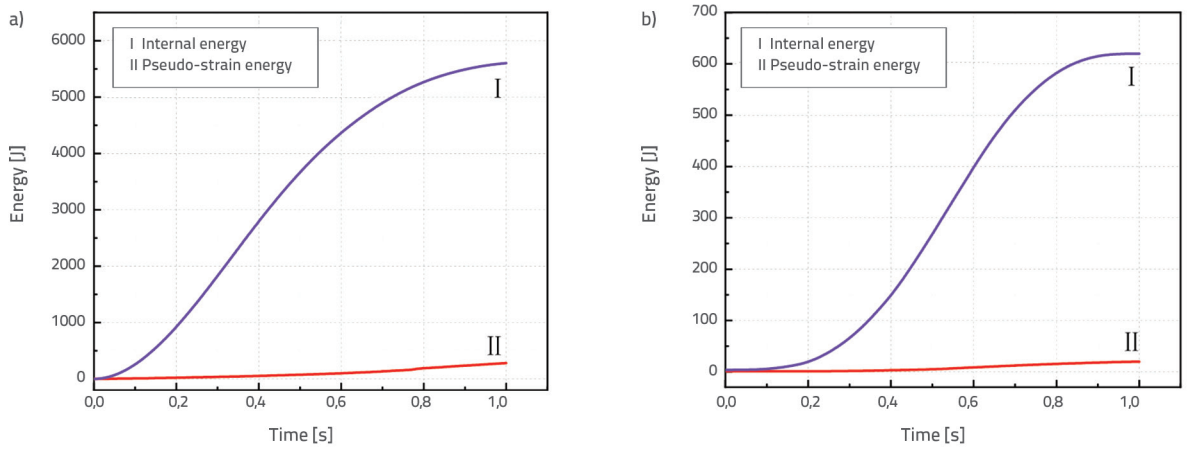

Figure 6. Energy-time histories analysis of two vehicle loadings: a) Energy history while vehicle loading; b) Energy history while concentrated loading at the vault

whereas the kinetic energy in the vault centralised loading failure simulation does not exceed 5.4 % of the internal energy. Additionally, the kinetic energy curve is similar to the internal energy curve within a 6 % error, which proves that the solution process remains in a quasi-static state. To avoid the problem of hourglassing during the simulation, the pseudo-strain energy should be controlled to less than 10 % of the internal energy. Figure 6 shows the pseudo-strain energy curves and internal energy curve for the two working conditions.

As shown in Figure 6, the pseudo-strain energy in the vehicle loading model accounts for approximately 4.9 % of the internal energy, and the pseudo-strain energy in the vault concentrated loading model accounts for approximately 3.2 % of the internal energy. This indicates the reliability and effectiveness of the finite element method.

3.3. Verification through the whole process of the loading condition

To further verify the effectiveness of the dynamic simulation of the cohesive model, Table 6 provides the results obtained by the simulation in this study (denoted as PRE in Tables 6 and 7) and Ref. [27] (denoted as REF in Table 6 and Table 7).

As shown in Table 6, the data from the simulation in this study matched the data from the loading test of the reference. Moreover, to make a clear comparison, two more calculated results of FEM, referred from the Cemetery Bridge, were selected [17] . One was established only with the bare arch (denoted as BAF in Table 7). The other was established with equivalent stuffing and without considering the contact relation of the different components (denoted by NCF in Table 7). Table 7 lists the ultimate load values of the solid web arch loading at the crown position.

Table 6. Calculation displacement comparison in different conditions

Working conditions	Maximum displacement [μm]					
	①*		②		③	
	REF	PRE	REF	PRE	REF	PRE
Half load left through half span	-48	-45	396	384	-8	-8
Half load left through full span	-66	-61	437	430	-30	-30
Half load right through half span	-28	-28	145	141	-15	-14
Half load right through full span	-36	-34	147	145	-3	-2
Full load left through half span	-58	-57	630	616	-64	-59
Full load left through full span	-76	-78	622	627	-56	-55
Full load right through half span	-51	-47	254	245	-20	-21
Full load right through full span	-46	-44	224	222	-23	-20
Note: * denotes the position label which is marked in the elevation graph of Figure 4.						

Table 7. Ultimate load value obtained by four methods

Results	BAF	NCF	PRE	REF
UBC [kN]	251	599	817	875

Table 8. The basic material properties of the model

Component	Yung's modulus [MPa]	Poisson ratio	Density [kg/m^3]
Masonry	5650	0.2	2500
Stuffing	500	0.3	1750
Abutment	1500	0.2	2400

If the results obtained from the field test (REF) were selected as standard values, the simulated errors of the BAF, NCF, and PRE were 71.3 % , 31.5 % , and 6.6 % , respectively. Compared with the models of bare arc or the model without considering the contact relation of different components, it is evident from the results that the cohesion model proposed in this study can accurately calculate the ultimate bearing capacity of the solid-web slab arch bridge.

4. Discussion of the influence of different factors on the ultimate bearing capacity

Following the modelling method of the Cemetery Bridge, a finite element model of a slab-arch bridge was established to study the influence of the impact factors on the ultimate bearing capacity, such as the thickness of the backfill, thickness of the arch ring, and rise-span ratio. An overview of 95 masonry arch bridges in the renovation project of rural highway bridges in Guangdong Province, east of northern China. Table 8 presents the basic material properties of the finite model, [28].
According to the trial calculation, the natural vibration period of the model is between 0.0625s and 0.0900s. On this basis, the operating time is still applied with 1.0 s in the following investigations.

4.1. Parametric analysis of different impact factors

To study the variation trend of the influence, the separation of variables method was adopted for these three impact factors, with an interval value of 0.1. With step-by-step loading, a

Table 9. Ultimate load value of the finite model under different conditions (unit: kN)

TAR [m]	RSR	TAS [m]				
		0.2	0.3	0.4	0.5	0.6
0.3	0.2	461.912	464.104	466.584	470.76	475.408
	0.25	488.992	506.92	524.072	529.024	534.84
	0.33	454.984	459.632	463.968	466.872	470.424
	0.5	359.256	367.312	375.240	393.168	409.784
0.4	0.2	462.612	465.392	467.916	473.080	477.832
	0.25	492.972	509.000	524.98	530.864	536.34
	0.33	455.984	461.400	465.484	468.128	472.932
	0.5	361.788	369.824	377.888	394.600	412.244
0.5	0.2	479.312	482.056	485.248	490.656	496.256
	0.25	512.952	527.632	541.888	547.448	553.840
	0.33	469.784	475.152	479.800	485.888	491.440
	0.5	380.32	388.280	396.536	413.8	430.704
0.6	0.2	502.668	507.000	510.656	515.720	520.808
	0.25	547.864	562.696	577.568	583.768	589.608
	0.33	494.92	500.116	505.216	510.808	516.484
	0.5	416.488	424.608	431.924	444.680	457.512
0.7	0.2	558.024	562.824	568.064	572.280	577.360
	0.25	614.776	629.72	645.248	651.536	657.376
	0.33	552.416	557.464	562.464	567.648	573.528
	0.5	484.656	491.928	499.312	507.560	516.320

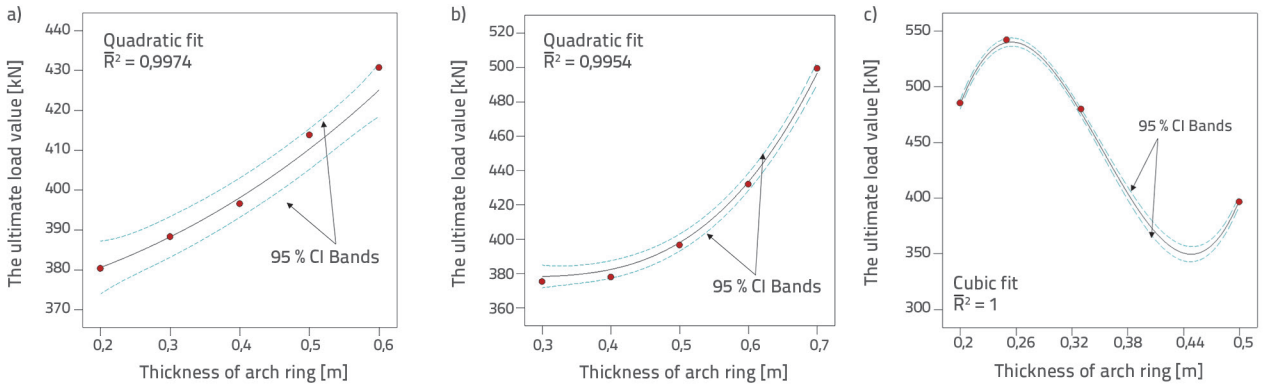

Figure 7. Variation trends of the ultimate load value under different conditions: a) Influence of the thickness of the arch backfill; b) Influence of the thickness of the arch ring; c) Influence of the rise-span ratio

linear load was applied in the bridge width direction at the crown position until the model showed a complete failure with the damage evolution proposed in Section 2. Table 9 lists the calculated results.

To reveal the relevant laws more clearly, two factors were adopted unchanged, while the third factor was changed with an interval of 0.1. Moreover, a polynomial fitting function was applied to reveal the relevant laws more clearly (Figure 7). Figure 7 illustrates that these three factors have a significant effect on the ultimate bearing capacity of slab-web arch bridges. In Figures 7(a)–8(d), the fitting curve of the thickness of the arch backfill and ring to the ultimate bearing capacity presents a quadratic function relationship. The average correlation coefficients reached 0.9974 and 0.9954 for each fitting model,

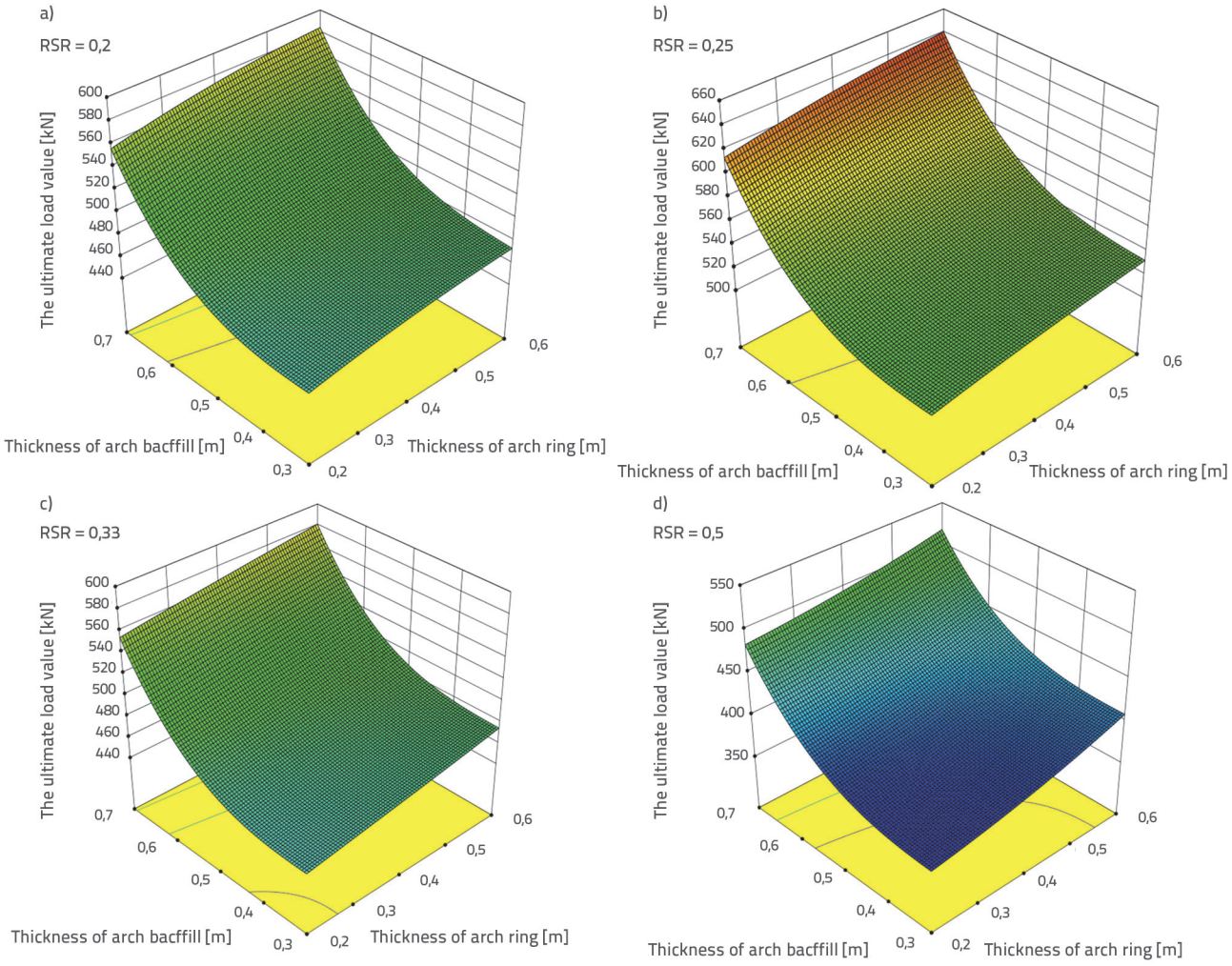

Figure 8. Response surface of these three factors ultimate load value, thickness of arch bacffill and thickness of arch ring: a) RSR = 0.2; b) RSR = 0.25; RSR = 0.33; d) RSR = 0.5

Table 10. Instruction of different working conditions

Shorthand	Instruction
W1	Perfect model while loading at the crown position
W2	Defect model at the 1/4 section while loading at the crown position
W3	Defect model at crown while loading at the crown position
W4	Perfect model with the bare arch

which further indicated that the fit was good. Otherwise, it is proved that the relationship between the rise and span ratio and the ultimate bearing capacity presents a standard cubic function relationship by 25 test data, while the average correlation coefficient has reached 1. Under the cubic relation, an optimal ratio exists with an average extreme point value of x = 0.2558 and a standard deviation of $\sigma = 5.75 \times 10^{-4}$. Once this condition is satisfied, the ultimate load value of the structure reaches its peak. To further discuss the influence of the thickness of the arch backfills and ring, Figure 8 shows a response surface analysis of these two influencing factors.

In Figure 8, the results of the response surface analysis show that the perfect prediction models of the thickness of the arch backfill and ring all monotonically increase under different rise-span ratios. The figures indicate that the backfill and arch ring will make the solid-web slab arch bridge evenly stressed. Additionally, it restrains the main arch ring to produce a tightening effect, and the stress concentration is avoided. Thus, the ultimate load value increased with an increase in the thickness of these two factors.

4.2. Influence analysis of the arch defects

Masonry arch bridges, especially those located on rural roads and built a long time ago, are not perfect. They all operate with different types of damage or defects. To analyse the influence of arch defects, structural damage analysis was performed by deleting the defective elements of the full bridge model under different conditions. The motion of the deleted elements indicates that the mass, damping, and load of the element change to zero. To clearly analyse the influence on the ultimate bearing capacity, three working conditions are presented in Table 10.

With the same material properties and actual size of the structure as in the previous study of this paper, the calculated results from two different sections of the bridge model are selected in Figure 9.

In Figure 9, the variation trend of any factor alone under W1–W3 is approximately the same as that of the research results in Section 4.2. In particular, the ultimate load value of each defect model was larger than that of the bare-arc model. Additionally, the defect model at the crown position has a greater impact on the structure and ultimate bearing value than that at the 1/4 section. The maximum, minimum, and average errors for W3–W1 were 33.7 % , 14.2 % , and 25 % , respectively. The maximum, minimum, and average errors of W2–W1 are 27.5 % , 6.5 % , and 16.2 % , respectively. It is illustrated that, owing to material weathering, building defects on the arch, and physical and chemical damage, the damage at the crown position has a greater impact on the ultimate bearing load of the structure than at the 1/4 section in actual engineering. From the overview, 65 % of solid-web slab arch bridges have defects in the vault position, and 35 % of them have defects near the 1/4 section. This further indicates that most of the current masonry arch bridges can still satisfy the existing operational requirements.

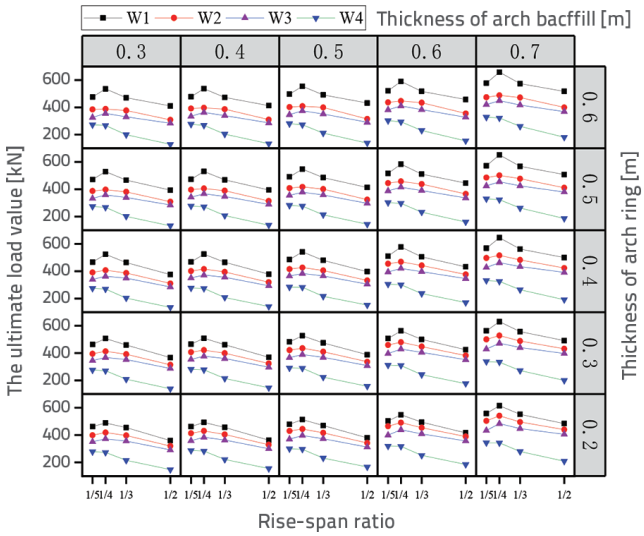

Figure 9. Variation trends of the ultimate load under different conditions

5. Conclusion

In this study, a dynamic zero-thickness cohesive element mode was established by considering the friction and interactions between different components. The validity and effectiveness of the model were verified by comparing its results with those of a previous study. The main conclusions of the explicit dynamic analysis are as follows:

- By considering the contribution of the arch backfills and the friction of the surface between different components, the proposed cohesive finite model can accurately simulate the dynamic behaviour of the solid-web arch bridge. Compared to the traditional simulation method that only considers a bare arch or equivalent stuffing, a large bearing capacity margin is still reserved in actual masonry bridges.
- The impact factors, such as the rise-span ratio, thickness of the arch ring, and backfills, all have a significant influence on the ultimate bearing capacity of solid-web arch bridges. The polynomial fitting function for the thickness of the arch ring and backfill showed a quadratic function relationship. Additionally, the polynomial fitting function of the rise-span

ratio exhibited a clear cubic function relationship. This further indicates that there exists an optional value *of f/l* = 1/3.909 to strengthen the structure under the same conditions.

- Under the same defect condition, the ultimate bearing load of the defective bridges at the crown position is generally 8.8 % larger than that at the 1/4 section in actual engineering. Considering the most defective position located at the vault through an overview of 95 masonry arch bridges, this further indicates that most of the current arch bridges can still meet the existing operational requirements despite the current rapid increase in traffic volume.
- The prediction model of MAS UBC formed by considering the strength of different materials and other parameters is the focus of future research.

Acknowledgments

Financial support from the Natural Science Basic Research Program of Shaanxi (Program No. 2020JQ-377) and the Fundamental Research Business Fees of Central Universities of Chang'an University (No. 310821161012) is gratefully acknowledged.

REFERENCES

[1] Huerta, S.: Galileo was wrong: The geometrical design of masonry arches, Nexus Netw., 8 (2006) 2, pp. 25-26

[2] Tóth, A.R., Orbán, Z., Bagi, K.: Discrete element analysis of a stone masonry arch, Mech. Res. Commun., 36 (2009), pp. 469–480

[3] Loureno, P.B., Krakowiak, K.J., Fernandes, F.M., et al: Failure analysis of Monastery of Jerónimos, Lisbon: How to learn from sophisticated numerical models, Engineering Failure Analysis, 14 (2007) 2, pp. 280-300

[4] Chetouane, B., Dubois, F., Vinches, M., Bohatier, C.: NSCD discrete element method for modelling masonry structures, Int. J. Numer. Methods Eng., 64 (2005), pp. 65–94

[5] Rafiee, A., Vinches, M.: Mechanical behaviour of a stone masonry bridge assessed using an implicit discrete element method, Engineering Structures, 48 (2013) 3, pp. 739-749

[6] Paul, A., Fanning, J., et al.: Three-dimensional modelling and full-scale testing of stone arch bridges – ScienceDirect, Computers & Structures, 79 (2001) 29, pp. 2645-2662

[7] Calió, I., Greco, A., D'Urso, D.: Structural models for the evaluation of eigen-properties in damaged spatial arches: a critical appraisal, Arch. Appl. Mech., 86 (2016), pp. 1853

[8] Cannizzaro, F., Greco, A., Caddemi, S., Calió, I.: Closed form solutions of a multi-cracked circular arch under static loads, Int. J. Solids. Struct., 121 (2017), pp. 191–200

[9] Calió, I., D'Urso, D., Greco, A.: The influence of damage on the eigen-properties of Timoshenko spatial arches, Comput. Struct., 190 (2017), pp.13–24

[10] Tóth, A.R., Orbán, Z., Bagi, K.: Discrete element analysis of a stone masonry arch, Mech. Res. Commun., 36 (2009) 4, pp. 469–80

[11] WeiXin, R., EHarik, I., George, E.: Blandford etc. Roebling suspension bridge. I:finite-elementmedoland free vibration response, H:ambient testing and live load response, Journal of Bridge Engineering, 9 (2004), 2, pp. 110-126

[12] Belytschko, T, Liu, V.Y., Moran, B.: Nonlinear Finite Element for Continua and structures, Monograph., John Wiley&Sons Inc., 2000.

[13] Cai, C., Shahawy, M.: Understanding Capacity Rating of Bridges from Load Tests, Practice Periodical on Structural Design and Construction, 8 (2003), 4, pp. 209-216

[14] Fang, N., Ellingwood, B., Zureick, A.: Bridge Rating Using System Reliability Assessment. II: Improvements to Bridge Rating Practices, Journal of Bridge Engineering, 16 (2011) 6, pp. 863-871

[15] Orduna, A., Lourenco, P.B.: Three-dimensional limit analysis of rigid blocks assemblages, Part I: torsion failure on frictional interfaces and limit analysis formulation, Int. J. Solids. Struct., 42 (2005), pp. 5140–5160

[16] Orduna, A., Lourenco, P.B.: Three-dimensional limit analysis of rigid blocks assemblages. Part II: load-path following solution procedure and validation, Int. J. Solids. Struct., 42 (2005), pp. 5161–5180

[17] Cannizzaro, F., Pantò, B., Caddemi, S., et al.: A Discrete Macro-Element Method (DMEM) for the nonlinear structural assessment of masonry arches, Engineering Structures, 168 (2018), pp. 243-256

[18] Tran, V.H., Vincens, E.: 2D-DEM modelling of the formwork removal of a rubble stone masonry bridge, Engineering Structures, 75 (2014), pp. 448-456

[19] Liang, F., Huang, M.: Structural Analysis of Solid Web Arch Bridge Considering the Confining Pressure Effect of Filling, Journal of Chongqing Jiaotong University (Natural Science), 29 (2010) 3, pp. 333-335

[20] Liang, L.: Analysis and Evaluation of Submerged Bearing Capacity of Stone Arch Bridge, Graduate thesis, Chongqing Jiaotong University, 2010.

[21] Baohua, X.: Evaluation of the bearing capacity of the in-service solid-web masonry arch bridge, Graduate thesis, Huazhong University of Science and Technology, 2013.

[22] Giulio, A.: On the influence of the shape of the interface law on the application of cohesive-zone models, Composites Science and Technology, 66 (2006), pp. 723-730

[23] MI, Y., Crisfield, M.A., Davies, G.A.O., et al.: Progressive delamination composite using interface elements, Journal of composite materials, 32 (1998), 14, pp.1246-1272

[24] Tubaldi, E., Macorini, L., Izzuddin, B.A.: Three-dimensional mesoscale modelling of multi-span masonry arch bridges subjected to scour, Eng Struct, 165 (2018); pp. 486–500

[25] Zhang, Y., Tubaldi, E., Macorini, L., Izzuddin, B.A.: Mesoscale partitioned modelling of masonry bridges allowing for arch-backfill interaction, Constr. Build. Mater., 173 (2018), pp. 820–842

[26] Boothby, T.E., Domalik, D.E., Dalal, V.A.: Service load response of masonry arch bridges, Journal of structural Engineering, 124 (1998) 1, pp. 17-23

[27] Abaqus 6.14: Online Documentation, Software Monograph, 2014.

[28] Chang'an University: Research Report on Technical Renovation Project of Dangerous Bridges in Rural Highways in Guangdong Province, 2021.